nature nanotechnology

REVIEW ARTICLE

PUBLISHED ONLINE: 27 NOVEMBER 2011 | DOI: 10.1038/NNANO.2011.196

Electrical contacts to one- and two-dimensional nanomaterials

François Léonard[1] and A. Alec Talin[2]

Existing models of electrical contacts are often inapplicable at the nanoscale because there are significant differences between nanostructures and bulk materials arising from unique geometries and electrostatics. In this Review, we discuss the physics and materials science of electrical contacts to carbon nanotubes, semiconductor nanowires and graphene, and outline the main research and development challenges in the field. We also include a case study of gold contacts to germanium nanowires to illustrate these concepts.

The high performance of modern electronics is a result of the fine control that has been achieved over the flow of charge carriers, beginning with charge injection into an active material through an electrical contact. Recognition of the importance of charge injection and extraction early in the history of semiconductors led to considerable efforts to engineer the properties of electrical contacts and to understand the basic science involved. More recently, researchers have explored the use of nanomaterials with unique electronic, optical, thermal and mechanical properties in place of conventional materials. Of these nanomaterials, carbon nanotubes, semiconductor nanowires and graphene have attracted the greatest interest, and many devices[1–5] have been demonstrated (Fig. 1). However, we will need a deeper understanding of the properties of electrical contacts at the nanoscale if devices made of nanotubes, nanowires and graphene are going to make the leap from the laboratory to real-world technology.

In this Review, we begin by discussing the alignment of electronic energy levels and bands at the interface between a metal and a nanostructure. We then address charge-injection phenomena, discuss various materials issues, and explore specific examples involving contacts to semiconductor nanowires. We conclude with a discussion of the challenges involved in the development of high-performance contacts to nanostructures, and the opportunities that would be opened up by the availability of such contacts.

First, however, we establish a central concept that is important when discussing contacts to nanostructures. The interface between the metal and the semiconductor in a conventional contact is planar. For nanocontacts however, there are multiple possible geometries, each with its unique properties. These can be divided into two main classes: end-bonded contacts and side contacts (Fig. 2). In the case of end-bonded contacts[6–8], the nanostructure abruptly ends at the contact, and atomic bonds are formed with the metal. End-bonded contacts are found in nanotubes and nanowires grown from catalyst metal particles, and in contacts formed by reacting carbon nanotubes[6] or nanowires[8] with metals. For side contacts, which are most often produced when metals are deposited on top of nanostructures, the nanostructure is embedded in the metal[9], and the bonding may be weak (that is, van der Waals) or strong, depending on the system under consideration.

Band alignment and band bending

An important concept in charge injection is the alignment of electronic energy levels at the interface between the metal and the nanostructure (Fig. 3). For semiconducting nanostructures, we are interested in the alignment between the conduction and valence bands in the semiconductor, and the Fermi level in the metal. If the energy of the Fermi level is in the gap between the valence and conduction bands of the semiconductor, there is a Schottky barrier ϕ_b at the interface (Fig. 3a). And if the Fermi level is either below the valence or above the conduction band edge, the contact is said to be ohmic (Fig. 3b). If the nanostructure is metallic, the presence of a tunnel barrier is a key issue (Fig. 3c).

The alignment of the Fermi level relative to the bandgap depends on many factors. The simplest model assumes that the Schottky barrier is given by $\phi_b = \Phi - \chi$, where Φ is the metal workfunction and χ is the semiconductor electron affinity. However, the interaction between the semiconductor and the metal can lead to the appearance of surface states with energies in the semiconductor bandgap and wavefunctions that decay exponentially into the semiconductor (Fig. 3d). A charge neutrality level is associated with these metal-induced gap states[10]. In general, the Fermi level will not be located at the charge neutrality level, thus creating a local charge in the semiconductor and an image charge in the metal. The electrostatic potential created by this dipole causes the valence and conduction bands to bend near the interface, and this tends to align the Fermi level with the charge neutrality level.

In bulk contacts, metal-induced gap states frequently determine completely the Schottky barrier, to such an extent that the metal workfunction often does not matter. However, in end-bonded[11] and side contacts to nanotubes and small nanowires[12], it has been suggested theoretically that metal-induced gap states have a much weaker impact on the band alignment due to electrostatics at reduced dimensions. Thus, one expects that the simple expression $\phi_b = \Phi - \chi$ will be a good description for some nanocontacts; this has been demonstrated experimentally in the case of contacts to carbon nanotubes[13,14] where it was demonstrated that Pd forms the best p-type contact. The approach has also been used to realize n-type contacts with low workfunction metals[15]. The case of end-bonded contacts to nanowires[16] will be discussed in a later section.

In the absence of Fermi-level pinning, the band alignment for side contacts is determined by the charge transfer between the metal and the nanostructure, which equilibrates the Fermi level across the two materials. The charge transferred to the nanostructure is screened by the metal, or equivalently, an image charge

[1]Sandia National Laboratories, Livermore, California, 94551, USA. [2]Center for Nanoscale Science and Technology, National Institute of Standards and Technology, Gaithersburg, Maryland, 20899, USA. *email: fleonar@sandia.gov; atalin@nist.gov

© 2011 Macmillan Publishers Limited. All rights reserved

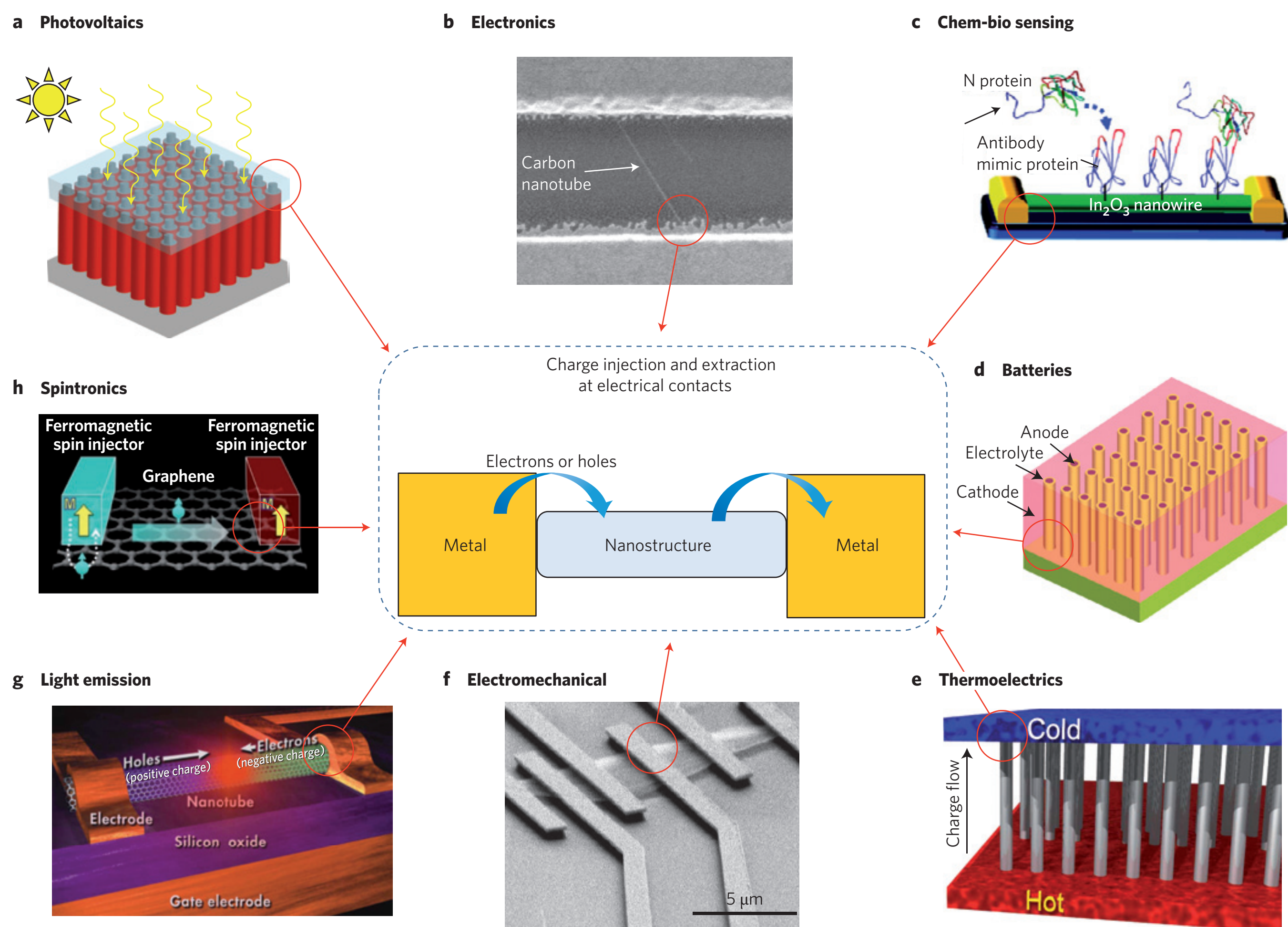

Figure 1 | Examples of nanomaterial-based devices. a, A photovoltaic device that uses an array of semiconducting nanowires (red) contacted by a transparent conductive top electrode. **b**, A carbon nanotube field-effect transistor. Current flow between source and drain electrodes (top and bottom, respectively) is controlled by a gate electrode (not shown). **c**, A chem-bio sensor using a nanowire functionalized with antibodies that bind to specific proteins, affecting the conductivity between two metallic electrodes. A third, gate electrode is also sometimes used in these devices. **d**, A three-dimensional Li-ion battery showing an array of anode nanowires (brown) coated with a thin solid electrolyte (gold) surrounded by a cathode matrix (pink). **e**, Thermoelectric power generation occurs when charge flows owing to a heat gradient, in this case along a nanowire array. The device can also be used for cooling, by forcing charge to flow in the other direction. **f**, A graphene nanoscale electromechanical system. A graphene membrane vibrates due to an oscillating gate voltage; the motion is detected by measuring the current flowing through the graphene. **g**, Light emission from a carbon nanotube device occurs when electrodes and holes injected from opposite electrodes meet and recombine. A gate electrode is used to tune the emission intensity. **h**, Graphene-based spintronics. One ferromagnetic metal contact injects spin-polarized charges into graphene, and a second ferromagnetic contact extracts the charge in a spin-dependent fashion. All of the devices shown rely on charge injection through a contact between a metal and a nanostructure. Panels reproduced with permission from: **a**, ref. 1, © 2009 AIP; **c**, ref. 2, © 2009 ACS; **d**, ref. 3, © 2008 ECS; **f**, ref. 4, © 2009 NPG; **g**, © IBM; **h**, Roland Kawakami, Univ. California, Riverside.

appears in the metal; the resulting charge dipole leads to an electrostatic potential difference between the metal and nanostructure, which shifts the bands of the nanostructure. The final band alignment is thus determined by the transferred charge and the difference in electrostatic potential; a way to consider this is in terms of the capacitance between the metal and the nanostructure. As an example, the capacitance between a metal and a carbon nanotube is large because of the small dimensions; thus the shift in potential is generally small, and the band alignment is determined mainly by the direct band alignment between the metal Fermi level and the nanotube bandgap[12]. A similar situation arises for semiconducting nanowires, where the potential shift is accommodated in the nanowire, but because of the small cross-section, the appropriate band bending cannot be established[12]. Graphene also displays charge transfer and re-alignment of the Fermi level when contacted by metals, an effect that also depends on the metal workfunction. Thus, contacts in graphene can be changed from p-type to n-type simply by using metals of different workfunctions[17].

Another important property of the metal/nanostructure interface is the band bending away from the contact. Whereas the band bending due to Fermi level pinning is a near-interface phenomenon, the doping in the semiconductor also leads to band bending, but on a length scale of tens of nanometres to micrometres. For bulk contacts, this length scale, called the depletion width (W, Fig. 3a) is given by $W = \sqrt{2\varepsilon\phi_b/ne}$ where ε is the dielectric constant, n is the dopant density, and e is the electron charge. This expression is appropriate for nanostructures as long as it gives a value of W that is less than the cross-section of the nanostructure, otherwise, the nanostructure dimensions alter the electrostatics

© 2011 Macmillan Publishers Limited. All rights reserved

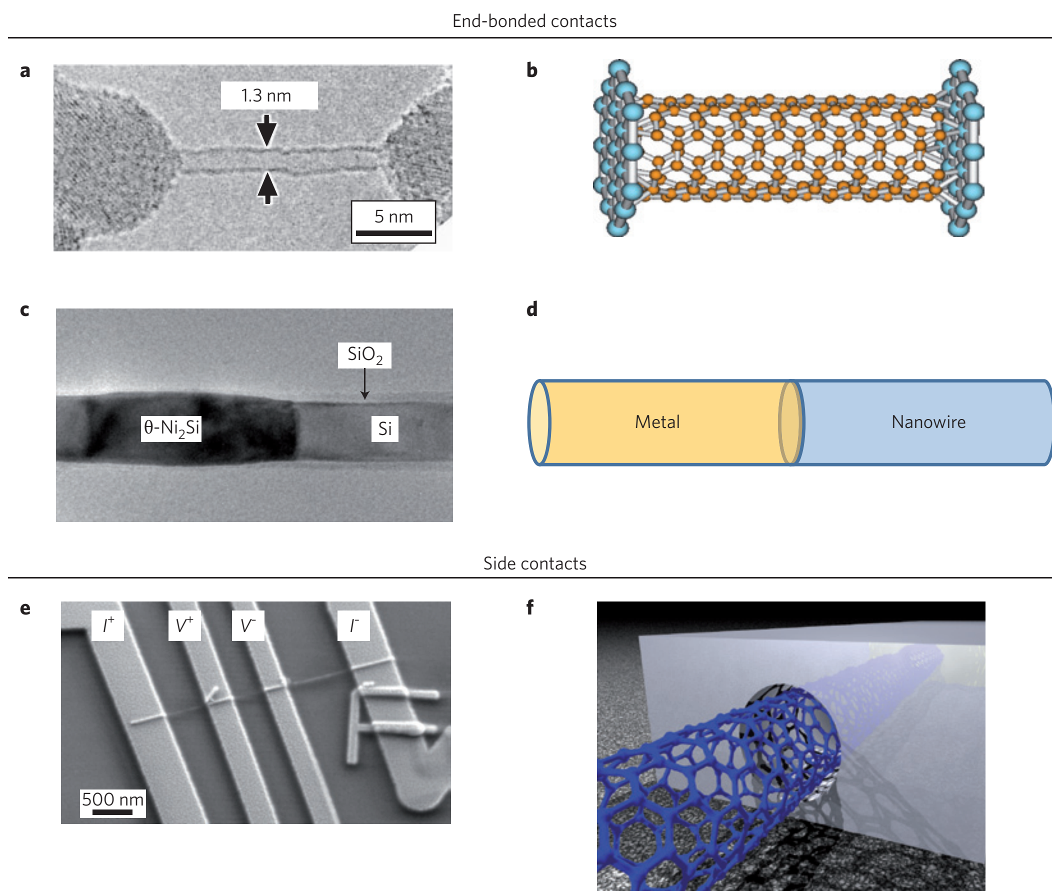

Figure 2 | Contact geometries. a-d, Two examples of end-bonded contacts to nanostructures. The top row shows a transmission electron micrograph image of a carbon nanotube end-bonded to Ti contacts (**a**), with a schematic atomic representation (**b**). The bottom row shows a scanning electron micrograph (SEM) image of a Si nanowire end-bonded to Ni_2Si (**c**) and a schematic (**d**). **e**,**f**, An example of a side contact to a nanostructure. A SEM mage shows a single carbon nanotube encapsulated by several electrodes (**e**), and an illustration shows the contact geometry (**f**). The four-probe geometry shown in (**e**) uses two electrodes to apply a voltage, and two electrodes to measure current, reducing the effect of contact resistance on the measurement. Panels reproduced with permission from: **a**, ref. 6, © 1999 AAAS; **b**, ref. 7, © 2003 APS; **c**, ref. 8, © 2008 AIP; **e**, ref. 9, © 2004 EDP.

and lead to a size-dependent W. In the case of carbon nanotubes, the cross-section is so small that only at very high doping is the bulk expression appropriate. In fact, at low and moderate doping levels, W is given by

$$W = R\exp(2\varepsilon_0\phi_b/\rho N_A R) \quad (1)$$

where ρ is the number of dopants per C atom, N_A is the number of C atoms per unit area, and R is the nanotube radius[18]. Thus, W is not only dependent on the radius but is extremely sensitive to the doping level and increases very rapidly at low doping concentrations. Experiments have confirmed the long-distance band bending in nanotubes[19]; a similar phenomenon also arises in graphene, where the band bending extends to hundreds of nanometres[20]. Modelling of end-bonded nanowires also demonstrated the diameter dependence of W (ref. 21). As will be discussed in the next section, the size of W plays an important role in determining the charge-injection processes that dominate the junction.

Charge injection

The band alignment concepts discussed in the previous section provide a basic picture of the electronic energy structure at electrical contacts. Charge injection can then be understood by describing charge-transport mechanisms through this energy landscape. In the presence of a Schottky barrier, the main transport mechanisms are thermionic emission, tunnelling through it, and electron–hole recombination in the depletion region (Fig. 4). In thermionic emission, electrons in the metal absorb thermal energy from phonons and are excited over the barrier, leading to an injection current that depends exponentially on voltage. In tunnelling, electrons quantum mechanically tunnel through the barrier, causing a charge-injection current that also depends exponentially on voltage, but is independent of temperature. In electron–hole recombination, electrons and holes are simultaneously injected in the depletion region, and recombine directly or through defects, with the possible emission of a photon.

In the case of carbon nanotubes, the electrical characteristics of field-effect transistors made with moderate workfunction metals that place the metal Fermi level in the nanotube bandgap (such as Ti) have been shown to be dominated by Schottky barriers. For such devices, the charge injection (and device function) is determined by tunnelling across the band bending at the metal–nanotube contacts, which is controlled by the gate. Mixed modes of charge injection where tunnelling and thermionic emission coexist are also possible, and have been observed in similar nanotube devices[22]. However, for many device applications, the presence of a Schottky barrier is detrimental to charge injection, and approaches to minimize its presence or impact are often sought.

One approach to overcome Schottky barriers at bulk metal–semiconductor junctions is to heavily dope the semiconductor

© 2011 Macmillan Publishers Limited. All rights reserved

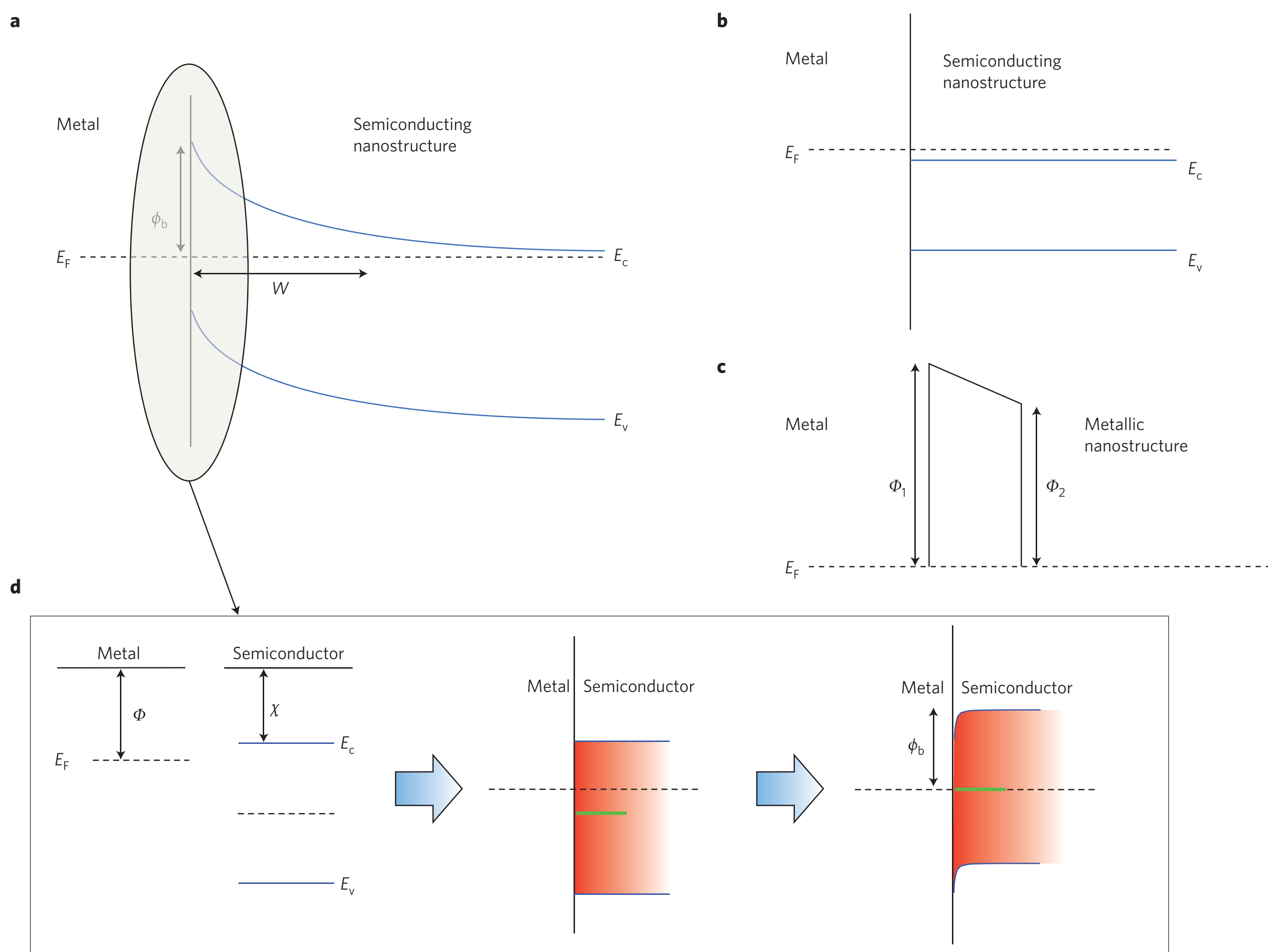

Figure 3 | Band alignment at metal/nanostructure interfaces. a, Band diagram for a Schottky contact, showing the top of the valence band (E_v), the bottom of the conduction band (E_c), the Fermi level (E_F), the Schottky barrier (ϕ_b) and the depletion width W. **b**, Band alignment for an n-type ohmic contact. **c**, For a contact between a metal and a metallic nanostructure, the presence of a tunnel barrier (with a profile that is determined by the workfunctions of the two metals Φ_1 and Φ_2) can govern the contact properties. **d**, In the simplest case, ϕ_b is determined by the difference between the metal workfunction Φ and the semiconductor electron affinity χ. However, in the near-interface region of a metal–semiconductor junction, interaction with the metal causes electronic states to appear in the bandgap of the semiconductor; associated with these states is a charge neutrality level denoted by the green line. In general, the metal Fermi level will not be at the charge neutrality level, and a local band bending can occur in the semiconductor to pin the Fermi level there.

near the contact to reduce W, allowing electrons to tunnel through the barrier. This approach is used extensively in modern semiconductor technology[23]. For end-bonded contacts to nanostructures, heavy doping can in principle work, because the necessary band bending, which occurs in the direction perpendicular to the metal/semiconductor interface, can be established along the length of the nanostructure. In the case of side contacts the situation is different, because the direction perpendicular to the metal/semiconductor interface is into the nanostructure cross-section, implying that W has to be smaller than the cross-section. Consequently, establishing the proper band bending is difficult, and requires increasingly more doping as the cross-section of the nanostructure decreases[12]. This leads to reduced tunnelling and rapidly increasing contact resistance as the nanowire diameter is reduced.

Electron–hole recombination is not usually the dominant transport mechanism at Schottky contacts. However, in some cases the height of the Schottky barrier is so large that both thermionic emission and tunnelling are negligible; a prominent example is that of contacts to Ge nanowires[16]. The Ge-nanowire/metal interface is dominated by very strong Fermi-level pinning that puts the Fermi level in the bandgap near the top of the valence band, regardless of the type of metal used. For n-type Ge, this leads to a large Schottky barrier for electrons of 0.59 eV, and little thermionic current. Charge injection is dominated by electron–hole recombination in the depletion region, but shows unusual properties compared with similar bulk injection: first, the recombination happens at the surface of the nanowire, leading to increased charge-injection efficiency for smaller-diameter nanowires. Second, the rapid increase of W with voltage at forward bias leads to a diameter-dependent ideality factor that deviates strongly from the bulk value. This case will be discussed in detail in a later section.

Another important aspect of charge injection that applies to side contacts is related to the length over which injection occurs from the contact edge, which is usually described with the contact transfer length L_T (Fig. 4). In contacts to bulk and thin-film materials, $L_T = \sqrt{\rho_c/R_S}$ where ρ_c is the contact resistivity and R_S is the sheet resistance under the contact. The transfer length determines

© 2011 Macmillan Publishers Limited. All rights reserved

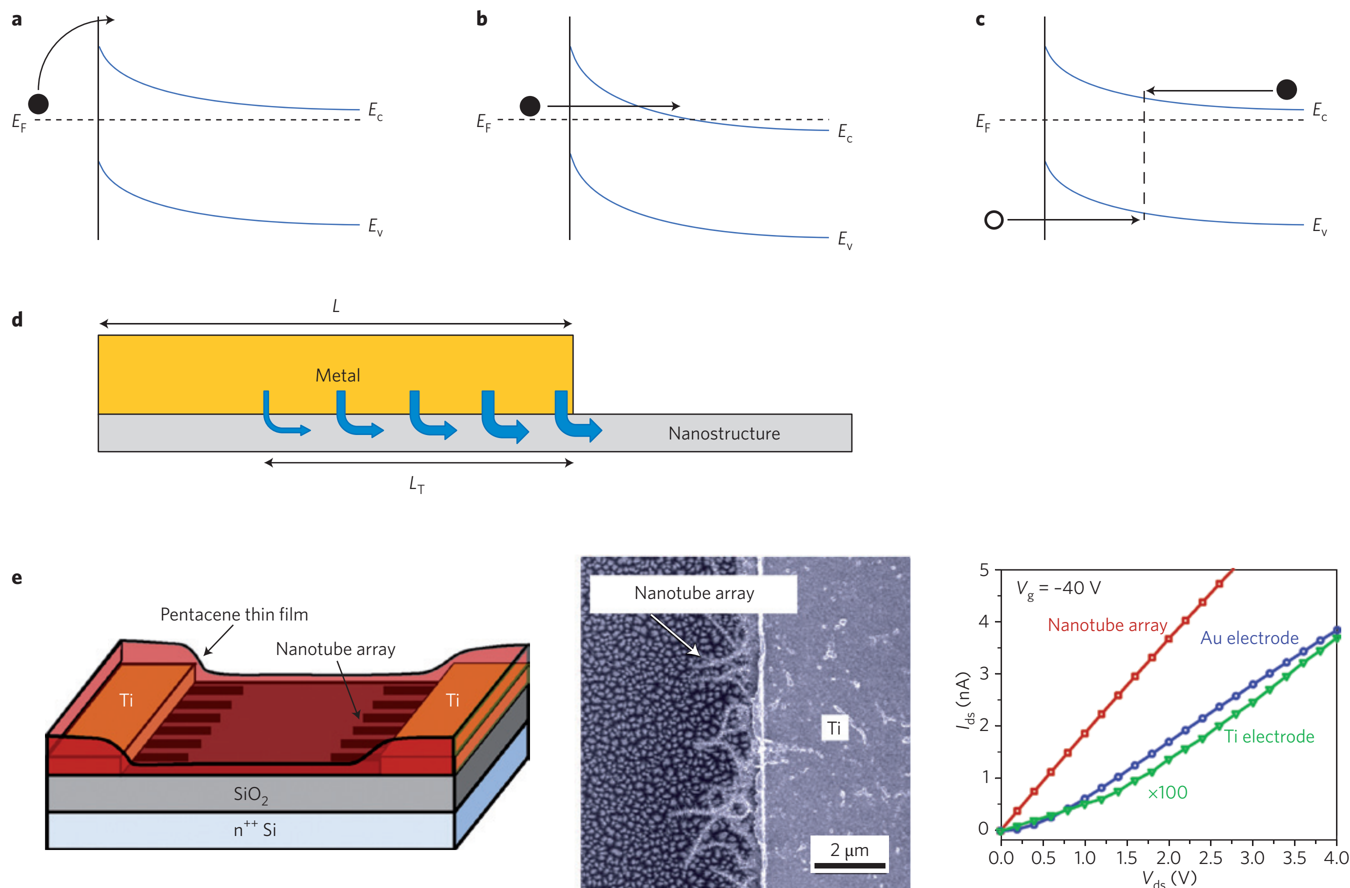

Figure 4 | Charge injection at metal–nanostructure contacts. a, Thermionic emission over a Schottky barrier. **b**, Tunnelling through a Schottky barrier. **c**, Electron–hole recombination in the depletion region (electrons and holes are represented by filled and open circles, respectively). **d**, The contact transfer length, L_T, is the length over which injection occurs from a metal that is side contacted to another material. **e**, Charge injection from metal electrodes into an organic thin film can be improved by attaching nanotube arrays to the electrodes, as shown in the left panel. The middle panel shows a transmission electron micrograph image of the attached tubes, and the right panel shows that the resulting source–drain current is higher than that measured when using bare Ti or bare Au electrodes. Panel **e** reproduced with permission from ref. 31, © 2009 ACS.

the contact resistance through the relation[24,25]

$$R_c = \sqrt{\rho_c R_S}\ \text{cotanh}\ (L/L_T)/L_W \tag{2}$$

where L is the length and L_W is the width of the contact. The charge transfer length is important not only for device performance, but also because it imposes limits on scaling and device densities.

Recent experimental work on Pd contacts to carbon nanotubes[26] studied the impact of contact length on contact resistance, and showed an inverse relationship, at least for contacts less than 300 nm in length. This behaviour is expected from equation (2) when $L << L_T$, thus providing a lower limit of 300 nm on L_T for this system. In the case of Ni contacts to graphene[27], a transfer length of 1 μm has been measured, whereas Pd gives much shorter transfer lengths in the 200–430 nm range[25]. (Note that the Pd–graphene contact resistance[25,28] has been found to depend on the gate voltage). Although these measurements support the notion of a contact transfer length, a key question is whether the formalism developed for bulk contacts (equation (2)) applies to nanocontacts more generally.

For example, theoretical work[29] has suggested that in the case of ballistic transport in metallic carbon nanotubes and graphene nanoribbons, the coupling strength with the metal determines L_T: strong coupling leads to small L_T, whereas weak coupling leads to large L_T. This is explained by the large perturbation that strong coupling imparts on the nanostructure at the edge of the contact, and the strong electron scattering that results, as opposed to weak coupling where the carriers can penetrate deeper in the contact. This idea has recently been extended to Pd contacts to graphene, where it was suggested that the carrier mean-free path under the metal and the metal–graphene coupling length are intimately tied to determine the contact resistance[28]. This is also borne out of analytical calculations for coaxial contacts to carbon nanotubes[30], and has been used to explain heating effects at metal–graphene contacts[25].

We close this section by discussing how nanostructures can be used to improve the charge-injection properties of the electrode itself. The idea is illustrated in Fig. 4e, where conventional electrodes are covered with carbon nanotubes that extend into the channel of a pentacene field-effect transistor. Because of their nanoscale dimensions, the electric field at the tips of the nanotubes is significantly enhanced compared with the planar metal-only electrode. This allows for very efficient charge injection into the organic material; in fact, without optimization, the charge-injection efficiency is 300 times as large in this example compared with the planar metal electrode[31]. This approach has recently been extended to charge injection in n-type organic transistors[32], and a related design was used as the source injection electrode in organic light-emitting diodes[33].

© 2011 Macmillan Publishers Limited. All rights reserved

NATURE NANOTECHNOLOGY DOI: 10.1038/NNANO.2011.196

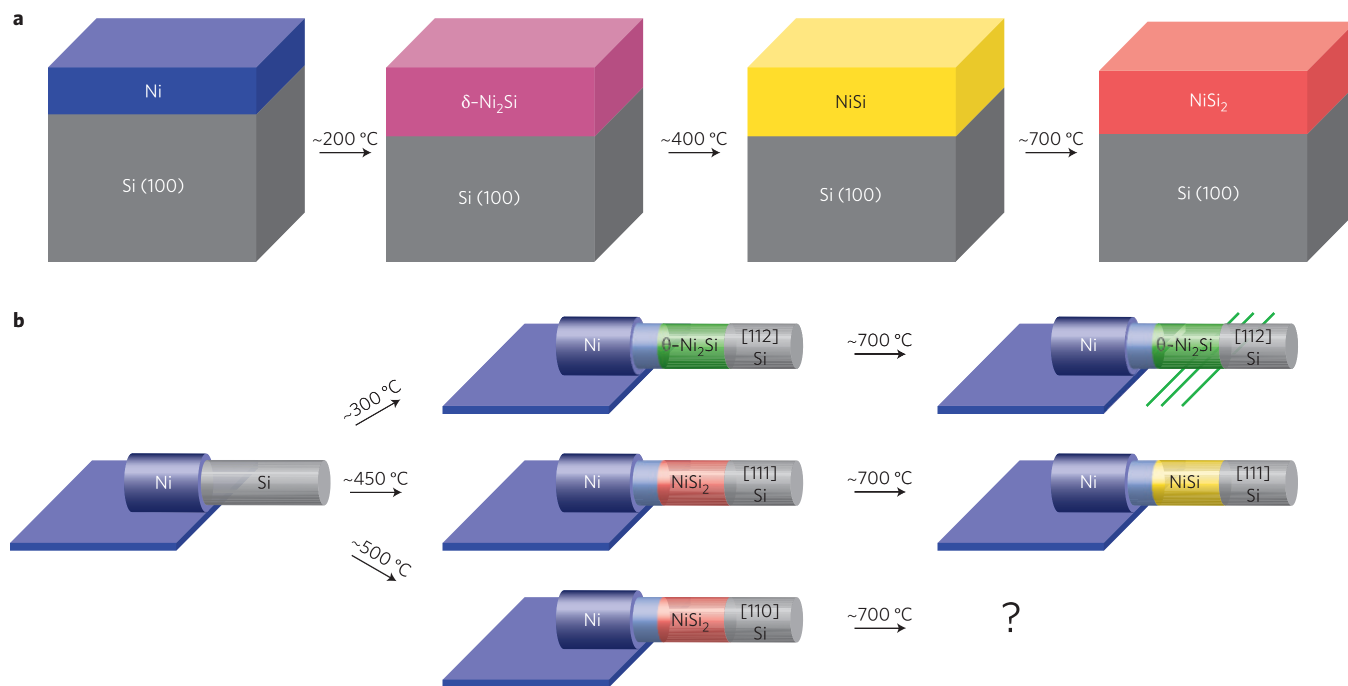

Figure 5 | Formation of the different phases of nickel silicide. a, Ni-silicides typically observed for a thin Ni film deposited on a (100) oriented Si wafer. As the annealing temperature is increased for a thin film on (100) Si, δ-Ni_2Si forms first owing to its large interdiffusion coefficient; NiSi forms at a higher temperature when all of the δ-Ni_2Si is consumed, and remains stable up to ~700 °C when the final phase, $NiSi_2$ begins to nucleate. **b**, The nickel silicides formed at contacts between Ni electrodes and Si nanowires depend on the crystallographic orientation of the nanowire. The presence of oxide on the nanowire surface and the starting amount of Ni can also affect the resulting silicide phase. For θ-Ni_2Si/(112)Si nanowires, outgrowing whiskers form above 700 °C owing to the high compressive stress[39].

Materials issues

Realizing contacts with reproducible and stable electrical characteristics requires precise control over the structure and composition of the metal/semiconductor interface. Improved contact metallization for bulk Si, Ge and compound semiconductor devices has been and continues to be the subject of intense research and development[23,34]. However, many of the schemes and processes developed for bulk devices have to be re-evaluated when applied to nanostructures because of their small volume, cross-sectional area, and large surface-to-volume ratio. This is particularly important for integrating nanostructures into high-performance electronics, where the source–drain series resistance increasingly becomes the limiting factor as other aspects of the device are optimized[35].

During the past decade NiSi replaced $TiSi_2$- and $CoSi_2$-based metallization in ultra-large-scale integrated Si circuits[36], owing to its superior scaling to linewidths <100 nm, lower annealing temperature and lower resistivity (~13 Ω cm versus ~18 Ω cm for $CoSi_2$), which means that similar sheet resistance can be achieved with thinner layers. The lower resistivity for NiSi, coupled with its lower density and smoother interfaces with Si (its formation mechanism is diffusion- rather than nucleation-limited) all add up to ~1/3 less Si consumption during contact formation, a critical advantage for contacting ultrathin Si-on-insulator device layers[37]. Planar-geometry NiSi-based contacts with specific resistance $<10^{-8}$ Ω cm^2 have been demonstrated[38], and Ni-silicide reactions have recently been explored for contacting Si nanowires[39–42]. These studies have revealed that Ni reactions with Si nanowires proceed differently than those for bulk Si devices (Fig. 5). Specifically, the nanowire crystallographic orientation and the nanowire's ability to better accommodate strain can lead to stabilization of silicide phases not normally observed in bulk or thin-film reactions under a similar heat treatment. These distinct silicide phases can impact device performance because of higher sheet resistivity and higher Schottky barriers, and can potentially lead to catastrophic device failure if large built-in stress leads to extended defect formation. When a thin Ni film is deposited onto a Si substrate and annealed, the phase with the highest interdiffusion coefficient, the orthorhombic δ-Ni_2Si, forms first, followed by NiSi, and finally $NiSi_2$ (ref. 36). NiSi is again the preferred phase for the same reasons given above. However, when Ni-silicide contacts are formed with [112]-oriented Si nanowires, the hexagonal θ-Ni_2Si phase forms around 300 °C, even though in the bulk this phase is not observed until 800 °C. Despite having over 5% difference in the in-plane bond lengths along at least one direction perpendicular to the metal/nanowire interface, this phase persists up to at least 600 °C; however, at 700 °C, the silicide forms outward-growing whiskers (which could short neighbouring devices) and a large number of twins owing to the large compressive stress[39]. With (111)-oriented Si nanowires (the most frequently observed growth direction) epitaxial $NiSi_2$ forms first and remains stable up to 700 °C, at which point the low-resistivity NiSi forms; however the monosilicide is expected to revert back to $NiSi_2$ at slightly higher temperatures, thus potentially leaving a very narrow process window for the preferred phase formation, and the possibility of agglomeration during the higher-temperature anneal.

Improved contact technology for Ge and group III–V compounds is currently an active area of research and development, spurred by the eventual need to replace Si with higher mobility semiconductors for high-performance CMOS (complementary metal-oxide semiconductor). However, few studies so far have focused on the contact metallurgy specific to nanowires made of these materials. Ni-germanides are similar in many respects to Ni-silicides and are currently being explored for contacting Ge nanowires[43]. The general strategy for making ohmic contacts to

© 2011 Macmillan Publishers Limited. All rights reserved

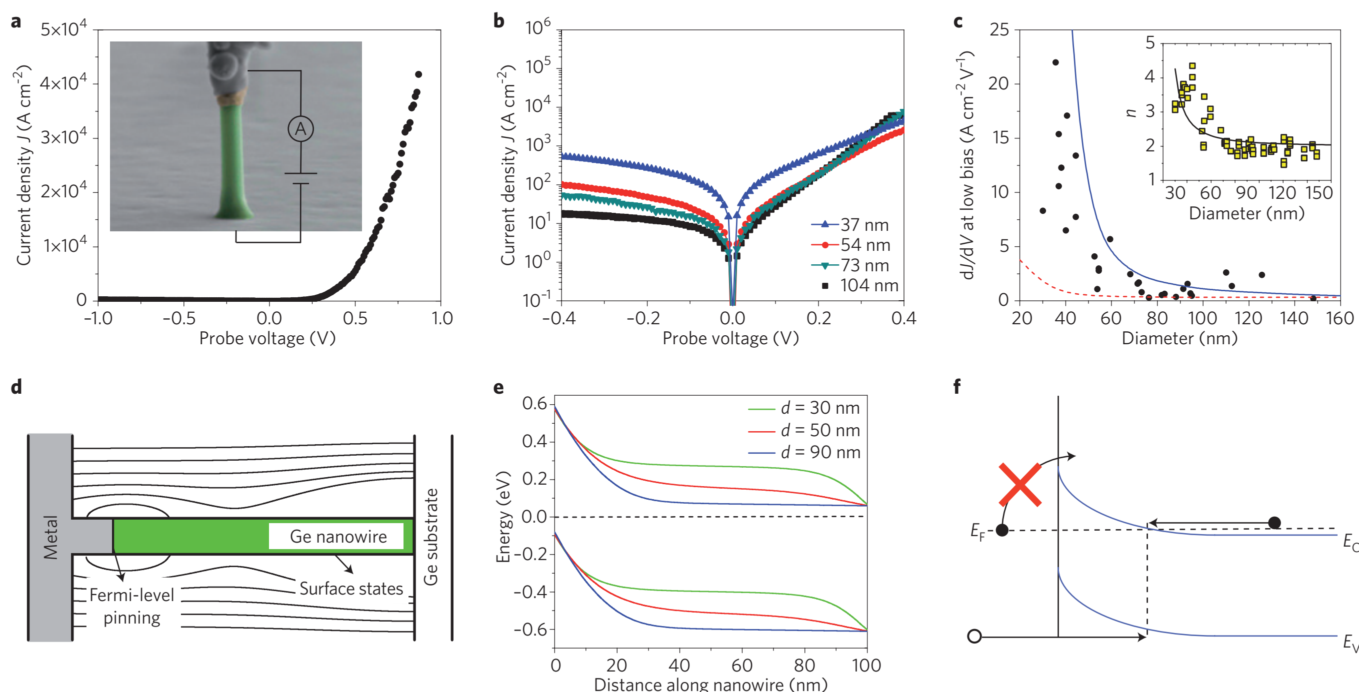

Figure 6 | Au-nanoparticle–Ge-nanowire contacts. a, Scanning electron microscopy image of a Ge nanowire (green) with a Au nanoparticle (brown) at its summit, contacted by a conducting probe (grey), and the resulting current–voltage curve. **b**, Measured current–voltage characteristics for nanowires of different diameters. **c**, Low bias conductance and ideality factor *n* (shown in the inset) as a function of diameter. The solid and dashed lines are calculated using a diameter-dependent and diameter-independent recombination time, respectively. **d**, Sketch of the system used for numerical simulations, showing electric field lines. **e**, Calculated band bending along the length of the nanowire for three nanowire diameters. The conduction band has positive energy, and the valence band negative energy. **f**, A large Schottky barrier prevents electron injection into the nanowire conduction band (left). Instead, charge injection is dominated by electron–hole recombination in the depletion region. Panels **a**–**e** reproduced with permission from ref. 16, © 2009 APS.

III–V and II–VI nanowires, provided these have a sufficiently high carrier concentration ($>\approx 10^{18}$ cm^{-3}), has been based on the use of Ti (ref. 44), or in some cases Al (ref. 45), both highly reactive metals with relatively low workfunctions, in combination with a low-resistivity metal such as Au. Specific contact resistances, however, have not been thoroughly investigated.

As already pointed out, another significant materials challenge to realizing metallic contacts to nanostructures with controlled electrical characteristics is the incorporation and activation of dopants. Bulk device-doping techniques such as ion implantation or solid-source in-diffusion lack the nanometre-scale depth and spatial resolution necessary for uniformly doping nanowires, and in the case of ion implantation, also result in significant lattice damage. A recent approach that addresses this problem takes advantage of the self-limiting nature of some Si surface reactions to assemble uniform, dopant-containing molecular monolayers on the nanowire surface[46]. Once annealed, the dopants diffuse into the bulk of the nanowire, and a dopant concentration as high as 10^{19} cm^{-3} within a depth of 20 nm was demonstrated. The dopant concentration is controlled by the packing density of the dopant precursor: a relatively small phosphate-containing molecule, 1-propylphosphonate, packs more densely and leads to approximately 10 times higher doping than the larger trioctylphosphine oxide.

Metal–carbon nanotube reactions have been attempted by high-temperature annealing of carbon nanotubes on Ti to form TiC and end-bonded contacts[6,47], but these contacts possess a large Schottky barrier approximately equal to half of the nanotube bandgap. Recently, however, it was reported that annealing carbon nanotubes contacted by Pt electrodes in vacuum above 900 K resulted in a sharp drop in contact resistivity[48]. These researchers used X-ray photoemission spectroscopy, Raman spectroscopy and electrochemical cyclic voltammetry to show that heating Pt in vacuum produced thin, graphitic carbon layers on the surface, or graphene nanodomains, which they argue increase the electronic overlap between the metal and the carbon nanotube, effectively increasing the area of the contact. This result opens interesting avenues for studying nanomaterials for charge injection into other nanostructures[49–51].

Case study on Au contacts to Ge nanowires

In this section, we consider Au contacts to Ge nanowires[16] to illustrate the practical aspects of the concepts discussed in the previous sections. Ge-nanowire growth by chemical vapour deposition with Au-catalyst nanoparticles on the substrate results in single-crystal Ge nanowires, with the Au catalyst nanoparticle remaining at the summit of the nanowire after growth (Fig. 6a, inset). Because the nanowires have diameters in the 30 nm to 150 nm range this provides a unique system for studying nanocontacts[16]. (A heavily-doped Ge substrate serves as the other, ohmic, contact). Atom-probe tomography measurements[52] and high-resolution transmission electron microscopy have indicated an abrupt interface between the Au-catalyst nanoparticle and the Ge nanowires[53].

Using a Au-coated tungsten scanning-tunnelling-microscope tip retrofitted inside of a scanning electron microscope (Fig. 6a, inset) individual Au–Ge nanocontacts can be directly probed, giving rectifying current–voltage characteristics[16] (Fig. 6a). The diode electrical behaviour is consistent with that observed at bulk Au/Ge interfaces[54], where a large Schottky barrier of 0.59 eV is present, and is nearly independent of the type of metal owing to strong Fermi-level pinning close to the Ge valence band. Our calculations show that this pinning of the Fermi level persists in the experimental nanowire geometry because of the high density of metal-induced gap states and the relatively large nanowire diameters.

© 2011 Macmillan Publishers Limited. All rights reserved

a Atomistic modelling

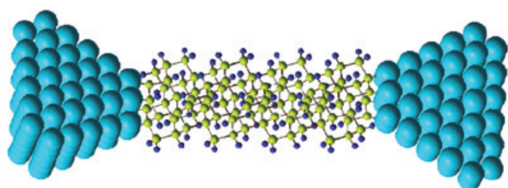

b Characterizing buried interfaces

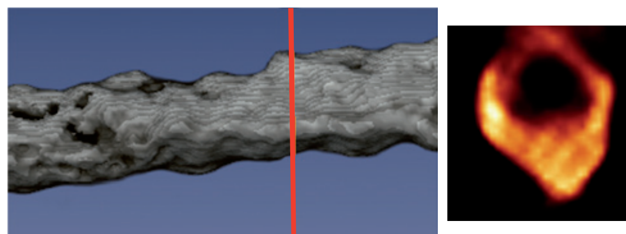

c Understanding and controlling doping

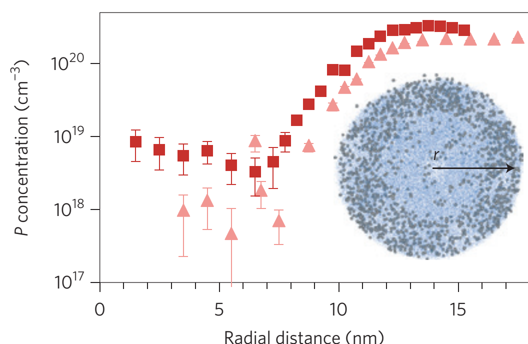

d Contacts to arrays

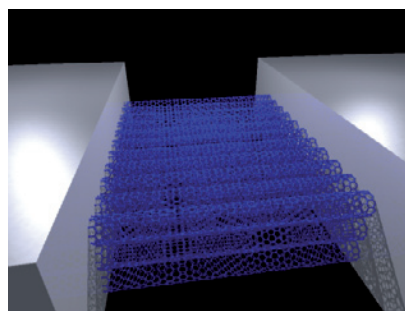

e New fabrication methodologies

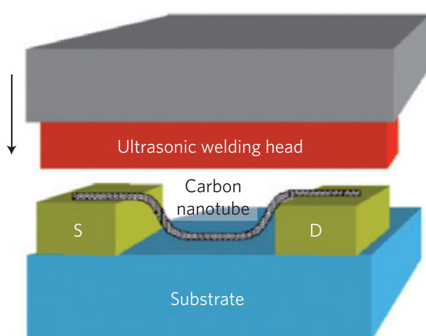

f Transparent contacts

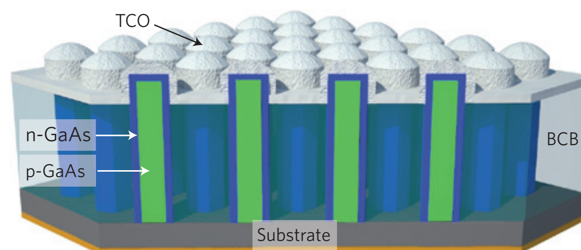

Figure 7 | Opportunities and challenges for research and development. a, Atomistic modelling of nanocontacts is needed to understand electronic and structural properties. The structure of an Al contact to a Si nanowire is illustrated. **b**, Experimental techniques to characterize the structural and electronic properties of buried interfaces can aid in understanding the behaviour of metal contacts to nanostructures. Electron tomography images show that a thin coating of Ti wets the carbon nanotube uniformly along its length (left panel) and in cross-section (right panel), preserving the shape of the nanotube. **c**, Experiments and theory are needed to understand dopant distribution in nanostructures. The panel shows a cross-sectional image of P dopants (grey dots) in a Ge (blue dots) nanowire obtained using atom probe tomography. The image and the measured dopant concentration shown in the main panel indicate that dopant distribution is nonuniform in the radial direction. Triangular points have a higher ratio of Ge:P precursors than the square points. **d**, New approaches are needed to make contacts to arrays of nanostructures. A carbon nanotube array is end-bonded at each end to metallic contacts. Alternatives include side contacts to the top layer of nanotubes or metal infiltration. **e**, New approaches for the fabrication of contacts include ultrasonic welding, which binds carbon nanotubes to electrodes, reducing the contact resistance. **f**, Transparent contacts to nanostructures are needed to enable photovoltaic devices, and can be made using transparent conducting oxides (TCO) such as indium tin oxide, as well as graphene or carbon nanotubes. A solar cell consisting of an ordered array of GaAs nanopillars with p-doped cores and n-doped shells, surrounded by a resin (benzocyclobutene, BCB) and contacted with a TCO is shown. Panels reproduced with permission from: **a**, ref. 66, © 2000 APS; **b**, ref. 60, © 2007 ACS; **c**, ref. 61, © 2009 NPG; **e**, ref. 62, © 2006 IOP; **f**, ref. 65, © 2011 ACS.

Figure 6b shows current–voltage curves for four other nanowires plotted on a log-normal plot, revealing a surprising observation: the current density at small bias increases with decreasing diameter, implying strong size effects in nanocontacts. To understand these results, we consider the main carrier-transport mechanisms characteristic of metal–semiconductor junctions that were introduced earlier: thermionic emission, tunnelling, recombination in the space–charge region, and recombination in the neutral region[55]. Tunnelling can be discounted as the main transport mechanism because W increases with decreasing diameter as we saw earlier; this would lower the tunnelling probability and decrease the current density. Thermionic emission, too, can be discounted, because of the zero-bias conductivity[55]

$$dJ/dV_{V=0} = (eA^*T^2/kT)\exp(-\phi_b/kT) \quad (3)$$

where A* is the Richardson's constant for Ge (50 A cm^{-2} K^{-2}), T is the temperature, k is the Boltzmann constant; ϕ_b is 0.59 eV here, giving a current density of ≈0.01 A cm^{-2}, that is orders of magnitude lower than what is observed experimentally. Recombination in

© 2011 Macmillan Publishers Limited. All rights reserved

the neutral region also gives a zero-bias conductivity that is at least two orders of magnitude too low. Thus, the only mechanism left is electron–hole recombination in the depletion region. This transport mechanism, which is frequently observed in situations with a relatively high Schottky barrier height and a low bandgap[56] as is true for Au–Ge contacts, is characterized by the expression

$$J = J_o\,[\exp(eV/nkT)-1] \tag{4}$$

where J_o depends on W, the minority recombination time τ, and the n-type dopant concentration N_d according to $J_0 = eN_dW/\tau$, and n is the so-called ideality factor, with $n = 2$ for electron–hole recombination in the depletion region in bulk contacts. The important point is that we expect an increase in W with decreasing diameter, and this is in qualitative accord with the results of Fig. 6c.

To test this idea, numerical calculations of the electron–hole recombination current using the Shockley–Read–Hall (SRH) recombination model[55] were performed[16]. The key to evaluating the conductivity from the SRH model is finding the electron and hole concentrations as a function of the distance along the nanowire. This can be achieved by numerically simulating[16] the nanowire electrostatics in the geometry of Fig. 6d. These calculations indicate that W increases from approximately 30 nm for a nanowire of diameter of 90 nm, to almost 100 nm for a nanowire of 30 nm diameter (Fig. 6e). Thus, the increase in junction conductivity with decreasing diameter can be partially accounted for by the increase in W; indeed, the dashed line in Fig. 6c represents the zero-bias conductivity calculated from equation (4) using the bulk recombination time. Although this can explain some of the increase, to account for the much larger increase in zero-bias conductivity observed experimentally, the dependence of the recombination time τ on the nanowire diameter has to be considered. Indeed, it is well known that unpassivated semiconductor surfaces represent excellent recombination sites. In nanowires, the surface-to-volume ratio increases as the diameter becomes smaller, thus leading to a dependence of the recombination time on the nanowire diameter[16]. With this diameter-dependent recombination time an excellent fit to the experimental data can be obtained (solid line in Fig. 6c), and yields a recombination velocity of 2×10^5 cm s^{-1}, in agreement with a value recently measured by ultrafast pump-probe spectroscopy on nanowires prepared in the same growth chamber[57]. More importantly, this example serves to illustrate how band alignment at the contact, electrostatics at reduced dimensions, and surface effects, come together to govern charge injection at nanocontacts (Fig. 6f).

Challenges and opportunities

To fully harness the properties of one- and two-dimensional nanomaterials, a better fundamental understanding of their properties is needed, as well as new approaches for realizing high-performance contacts (Fig. 7). This requires new theoretical and experimental insights. For example, most existing models for the electronic properties of metal–nanostructure contacts assume that the electronic structure of the nanomaterials is unaffected, or only slightly disturbed, by the presence of the metal. However, this may not be the case, because the metal provides a new type of screening environment that could substantially impact the electronic properties. Indeed, the electron–electron interaction depends sensitively on the dielectric response of the system, and recently it was demonstrated through many-body *ab initio* approaches that the presence of acoustic plasmons in one-dimensional materials can significantly renormalize the bandgap[58]. Fundamental research is needed to develop and implement such many-body approaches in the context of contacts.

A related situation would be that of superconducting contacts to nanostructures[59], where theoretical insight and computational modelling are needed to understand the impact of the superconducting metal on the nanostructure properties. To validate these computational approaches, it is necessary to experimentally measure the electronic, structural and chemical properties of the contacts. For example, in side contacts the metal needs to form a conformal coating on the nanostructure without the presence of impurities. Characterizing such interfaces is a challenge because of the small contact area for end-bonded contacts, and because the nanomaterial is embedded in the metal for side contacts. The latter is a particularly acute problem, and only recently has progress been made in using scanning tunnelling electron microscopy to image the structure of nanotubes embedded in a metal[60]; further work is needed to improve the spatial resolution and to obtain information on the electronic structure.

As we have seen in earlier sections, an important aspect of contacts is the control of doping in the semiconductor. For bulk contacts, procedures have been developed (for example, ion implantation) and refined to precisely control contact properties. The understanding of dopant properties in nanostructures has not reached this level of understanding. For example, it is only recently that the dopants in nanowires have been imaged using atom-probe tomography[61], revealing that their spatial distribution is non-uniform. Thus, understanding the role of non-uniform dopant distribution on contact properties and the origin of this distribution is essential, as are developing approaches to control it.

However, a fundamental understanding of contact properties alone will not be sufficient to bring nanoscale devices from the laboratory to real-world technology. For this to happen, rapid, repeatable and reliable contact formation needs to be achieved. Although much discussion has focused on devices using individual nanostructures, many technological implementations will require arrays or thin films of nanostructures. The challenge there is that conventional deposition of metals on the array would only contact the top layer of the array or film, necessitating hopping between the individual nanostructures to transport the injected current.

A better approach may be to contact all the nanostructures directly with the metal. Some approaches developed in the context of individual nanostructures may provide a path in this direction. For example, recent work has shown that ultrasonic welding, whereby a welding head vibrating at ultrasonic frequencies is used to bond materials together, can be applied to carbon nanotube contacts with metals[62]. The vibrational energy is sufficient to induce a reaction between the nanotube and the metal, essentially melting the two together. A related high-temperature process has also been implemented for contacts to individual carbon nanotubes, whereby Ti is reacted with the nanotube to form TiC (ref. 6); an intriguing question is whether this can be applied to arrays or thin films. As for graphene, recent work has demonstrated that oxygen plasma treatment before metal deposition cleans away photoresist residue and creates defects that significantly lower the contact resistance, making the interface insensitive to the metal workfunction[63].

Transparent contacts are another important technology area, being critical for solar-cell applications. Although nanomaterials have been studied as a replacement for existing transparent contact materials, a different question is how to make the transparent contacts to the active area of a solar cell made of nanomaterials. A specific example would be arrays of vertical nanowires, which require a top transparent contact; research and development work is needed to understand the structural properties of such contacts and the band alignment, as well as to develop fabrication approaches to realize high-performance contacts. Work in this direction has already demonstrated that conventional transparent contact materials such as indium tin oxide can be used to realize nanowire-array solar cells with reasonable energy conversion efficiencies[64,65].

Metallic contacts to nanostructures therefore represent both challenges and opportunities. The unique characteristics of charge

© 2011 Macmillan Publishers Limited. All rights reserved

injection and extraction that arise from reduced dimension and scale need to be completely understood for nanomaterials to continue to transition from research to real applications. These unique characteristics include electrostatics (with effects on barrier heights and depletion widths), surface effects (with effects on charge-recombination rates), geometry and alignment, and fabrication and materials requirements. At the same time, this unique behaviour will also allow compelling new device designs and fabrication approaches that strengthen the argument for the use of nanomaterials in the first place.

Corrected online: 28 November 2011

References

1. Peters, C. H., Guichard, A. R., Hryciw, A. C., Brongersma, M. L. & McGehee, M. D. Energy transfer in nanowire solar cells with photon-harvesting shells. *J. Appl. Phys.* **105,** 124509 (2009).
2. Ishikawa, F. N. *et al.* Label-free, electrical detection of the SARS virus N-protein with nanowire biosensors utilizing antibody mimics as capture probes. *ACS Nano* **5,** 1219–1224 (2009).
3. Dunn, B., Long, J. W. & Rolison, D. R. Rethinking multifunction in three dimensions for miniaturizing electrical energy storage. *Electrochem. Soc. Interface* **17,** 49–53 (2008).
4. Chen, C. *et al.* Performance of monolayer graphene nanomechanical resonators with electrical readout. *Nature Nanotech.* **4,** 861–867 (2009).
5. Misewich, J. A., Martel, R., Avouris, Ph., Tsang, J. C., Heinze, S. & Tersoff, J. Electrically induced optical emission from a carbon nanotube FET. *Science* **300,** 783–786 (2003).
6. Zhang, Y., Ichihashi, T., Landree, E., Nihey, F. & Iijima, S. Heterostructures of single-walled carbon nanotubes and carbide nanorods. *Science* **285,** 1719–1722 (1999).
7. Palacios, J. J., Pérez-Jiménez, A. J., Louis, E., SanFabían, E. & Vergés, J. A. First principles phase-coherent transport in metallic nanotubes with realistic contacts. *Phys. Rev. Lett.* **90,** 106801 (2003).
8. Woodruff, S. M. *et al.* Nickel and nickel silicide Schottky barrier contacts to n-type silicon nanowires. *J. Vac. Sci. Technol. B* **26,** 1592–1596 (2008).
9. Zhang, Z., Dikin, D. K., Ruoff, R. S. & Chandrasekhar, V. Conduction in carbon nanotubes through metastable resonant states. *Europhys. Lett.* **68,** 713–719 (2004).
10. Tersoff, J. Schottky barrier heights and the continuum of gap states. *Phys. Rev. Lett.* **52,** 465–468 (1984).
11. Léonard, F. & Tersoff, J. Role of Fermi-level pinning in nanotube Schottky diodes. *Phys. Rev. Lett.* **84,** 4693–4696 (2000).
12. Léonard, F. & Talin, A. A. Size-dependent effects on electrical contacts to nanotubes and nanowires. *Phys. Rev. Lett.* **97,** 026804 (2006).
13. Chen, Z., Appenzeller, J., Knoch, J., Lin, Y.-M. & Avouris, Ph. The role of metal-nanotube contact in the performance of carbon nanotube field-effect transistors. *Nano Lett.* **5,** 1497–1502 (2005).
14. Kim, W. *et al.* Electrical contacts to carbon nanotubes down to 1 nm in diameter. *Appl. Phys. Lett.* **87,** 173101 (2005).
Refs 13 and 14 reported the experimental demonstrations that the band alignment at metal–nanotube contacts depended on the nanotube diameter.
15. Wang, C., Ryu, K., Badmaev, A., Zhang, J. & Zhou, C. Metal contact engineering and registration-free fabrication of complementary metal-oxide semiconductor integrated circuits using aligned carbon nanotubes. *ACS Nano* **5,** 1147–1153 (2011).
16. Léonard, F., Talin, A. A., Swartzentruber, B. S. & Picraux, S. T. Diameter-dependent electronic transport properties of Au-catalyst/Ge-nanowire Schottky diodes. *Phys. Rev. Lett.* **102,** 106805 (2009).
17. Giovannetti, G. *et al.* Doping graphene with metal contacts. *Phys. Rev. Lett.* **101,** 026803 (2008).
18. Léonard, F. *The Physics of Carbon Nanotube Devices* (William Andrew, 2008).
19. Bachtold, A., Hadley, P., Nakanishi, T. & Dekker, C. Logic circuits with carbon nanotube transistors. *Science* **294,** 1317–1320 (2001).
20. Mueller, T., Xia, F., Freitag, M., Tsang, J. & Avouris, Ph. Role of contacts in graphene transistors: a scanning photocurrent study. *Phys. Rev. B* **79,** 245430 (2009).
21. Hun, J., Liu, Y., Ning, C. Z., Dutton, R. & Kang, S-M. Fringing field effects on electrical resistivity of semiconductor nanowire-metal contacts. *Appl. Phys. Lett.* **92,** 083503 (2008).
22. Appenzeller, J., Radosavljevic, M., Knoch, J. & Avouris, Ph. Tunneling versus thermionic emission in one-dimensional semiconductors. *Phys. Rev. Lett.* **92,** 048301 (2004).
23. Brillson, L. J. *Contacts to Semiconductors: Fundamentals and Technology* (Noyes, 1993).
24. Reeves, G. K. & Harrison, H. B. Obtaining the specific contact resistance from transmission line model measurements. *IEEE Electron Dev. Lett.* **3,** 111–113 (1982).
25. Grosse, K. L., Bae, M.-H., Lian, F., Pop, E. & King, W. P. Nanoscale Joule heating, Peltier cooling and current crowding at graphene-metal contacts. *Nature Nanotech.* **6,** 287–290 (2011).
26. Franklin, A. D. & Chen, Z. Length scaling of carbon nanotube transistors. *Nature Nanotech.* **5,** 858–862 (2010).
This paper demonstrates scaling of the contact length, and also scaling of the channel length down to 15 nm.
27. Nagashio, K., Nishimura, T., Kita, K. & Toriumi, A. Contact resistivity and current flow path at metal/graphene contacts. *Appl. Phys. Lett.* **97,** 143514 (2010).
28. Xia, F., Pereibenos, V., Lin, Y.-M., Wu, Y. & Avouris, Ph. The origins and limits of metal-graphene junction resistance. *Nature Nanotech.* **6,** 179–184 (2011).
29. Nemec, N., Tománek, D. & Cuniberti, G. Contact dependence of carrier injection in carbon nanotubes: an *ab initio* study. *Phys. Rev. Lett.* **96,** 076802 (2006).
30. Solomon, P. Contact resistance to a one-dimensional quasi-ballistic nanotube/wire. *IEEE Electron Dev. Lett.* **32,** 246–248 (2011).
31. Aguirre, C. M., Ternon, C., Paillet, M., Desjardins, P. & Martel, R. Carbon nanotubes as injection electrodes for organic thin film transistors. *Nano Lett.* **9,** 1457–1461 (2009).
32. Cicoira, F., Aguirre, C. M. & Martel, R. Making contacts to n-type organic transistors using carbon nanotube arrays. *ACS Nano* **5,** 283–290 (2011).
33. McCarthy, M. A. *et al.* Low-voltage, low-power, organic light-emitting transistors, for active matrix displays. *Science* **332,** 570–573 (2011).
34. Dimoulas, A., Toriumi, A. & Mohney, S. E. Source and drain contacts for germanium and III-V FETs for digital logic. *MRS Bull.* **34,** 522–529 (2009).
35. King, T-J. Taking silicon to the limit. *Electrochem. Soc. Interface* **14,** 38–42 (2005).
36. Lavoie, C., d'Heurle, F. M., Detavernier, C. & Cabral, C. Towards implementation of a nickel silicide process for CMOS technologies. *Microelec. Eng.* **70,** 144–157 (2003).
This article details the morphology, composition and resistivity of Ni thin films reacting with Si, and explains why NiSi became the preferred metallization.
37. Ahn, C-G. *et al.* A two-step annealing process for Ni silicide formation in an ultra-thin body RF SOI MOSFET. *Mater. Sci. Eng. B* **147,** 183–186 (2008).
38. Zhang, Z. *et al.* Sharp reduction in contact resistivities by effective Schottky barrier lowering with silicides as diffusion sources. *IEEE Electron Dev. Lett.* **31,** 731–733 (2010).
39. Dellas, N. S. *et al.* Orientation dependence of nickel silicide formation in contacts to silicon nanowires. *J. Appl. Phys.* **105,** 094309 (2009).
This article describes the real-time observation (with a transmission electron microscope) of Ni reactions with Si nanowires as a function of anneal temperature.
40. Lin, Y-C., Chen, Y., Xu, D. & Huang, Y. Growth of nickel silicides in Si and Si/SiOx core/shell nanowires. *Nano Lett.* **10,** 4721–4726 (2010).
41. Hong, S. H. *et al.* Electrical characteristics of nickel silicide–silicon heterojunction in suspended silicon nanowires, *Solid State Electron* **56,** 130–134 (2011).
42. Motayed, A. *et al.* Correlation between the performance and microstructure of Ti/Al/Ti/Au Ohmic contacts to p-type silicon nanowires. *Nanotechnology* **22,** 075206 (2011).
43. Dellas, N. S., Minassian, S., Redwing, J. M. & Mohney, S. E. Formation of nickel germanide contacts to Ge nanowires. *Appl. Phys. Lett.* **97,** 263116 (2010).
44. Talin, A. A., Wang, G. T., Lai, E. & Anderson, R. J. Correlation of growth temperature, photoluminescence, and resistivity in GaN nanowires. *Appl. Phys. Lett.* **92,** 093105 (2008).
45. Lee, T. I. *et al.* Electrical contact tunable direct printing route for a ZnO nanowire Schottky diode. *Nano Lett.* **10,** 3517–3523 (2010).
46. Ho, J. C. *et al.* Controlled nanoscale doping of semiconductors via molecular monolayers. *Nature Mater.* **7,** 62–67 (2008).
47. Martel, R. *et al.* Ambipolar electrical transport in semiconducting single-wall carbon nanotubes. *Phys. Rev. Lett.* **87,** 256805 (2001).
48. Kane, A. A. *et al.* Graphitic electrical contacts to metallic single-walled carbon nanotubes using Pt electrodes. *Nano Lett.* **9,** 3586–3591 (2009).
49. Jang, S. *et al.* Flexible, transparent single-walled carbon nanotube transistors with graphene electrodes. *Nanotechnology* **21,** 425201 (2010).
50. Li, B. *et al.* All-carbon electronic devices fabricated by directly grown single-walled carbon nanotubes on reduced graphene oxide electrodes. *Adv. Mater.* **22,** 3058–3061 (2010).
51. Aikawa, S. *et al.* Facile fabrication of all-SWNT field-effect transistors. *Nano Res.* **4,** 580–588 (2011).
52. Perea, D. E., Wijayaa, E., Lensch-Falk, J. L., Hemesath, E. R. & Lauhon, L. J. Tomographic analysis of dilute impurities in semiconductor nanostructures. *J. Solid State Chem.* **181,** 1642–1649 (2008).

© 2011 Macmillan Publishers Limited. All rights reserved

53. Taraci, J. L. *et al.* Nanopillar growth mode by vapor-liquid-solid epitaxy. *Appl. Phys. Lett.* **84,** 5302–5304 (2004).
54. Nishimura, T., Kita, K. & Toriumi, A. Evidence for strong Fermi level pinning due to gap states at metal/germanium interface. *Appl. Phys. Lett.* **91,** 123123 (2007).
55. Sze, M. & Ng, K. K. *Physics of Semiconductor Devices* 3rd edn (Wiley 2007).
56. Rhoderick, E. H. & Williams, R. H. *Metal–Semiconductor Contacts* 2nd edn (Oxford Science, 1988).
57. Prasankumar, R. P., Choi, S., Trugman, S. A., Picraux, S. T. & Taylor, A. J. Ultrafast electron and hole dynamics in germanium nanowires. *Nano Lett.* **8,** 1619–1624 (2008).
58. Spataru, C. D. & Léonard, F. Tunable bandgaps and excitons in doped carbon nanotubes made possible by acoustic plasmons. *Phys. Rev. Lett.* **104,** 177402 (2010).
59. Simizu, M., Akimoto, H. & Ishibashi, K. Electronic transport of single-wall carbon nanotubes with superconducting contacts. *Jpn. J. Appl. Phys.* **50,** 035102 (2011).
60. Cha, J. J. *et al.* Three-dimensional imaging of carbon nanotubes deformed by metal islands. *Nano Lett.* **7,** 3770–3773 (2007).
61. Perea, D. E. *et al.* Direct measurement of dopant distribution in an individual vapor–liquid–solid nanowire. *Nature Nanotech.* **4,** 315–319 (2009). **The first report of spatially resolved measurements of dopant distribution in nanowires**.
62. Chen, C., Yan, L., Kong, E. S-W. & Zhang, Y. Ultrasonic nanowelding of carbon nanotubes to metal electrodes. *Nanotechnology* **17,** 2192–2197 (2006).
63. Robinson, J. A. *et al.* Contacting graphene. *Appl. Phys. Lett.* **98,** 053103 (2011).
64. Czaban, J. A., Thompson, D. A. & LaPierre, R. R. GaAs core-shell nanowires for photovoltaic applications. *Nano Lett.* **9,** 148–154 (2009).
65. Mariani, G. *et al.* Patterned radial GaAs nanowire solar cells. *Nano Lett.* **11,** 2490–2494 (2011).
66. Landman, U., Barnett, R. N., Scherbakov, A. G. & Avouris, Ph. Metal-semiconductor nanocontacts: Silicon nanowires. *Phys. Rev. Lett.* **85,** 1958–1961 (2000).

Acknowledgements

F.L. acknowledges financial support from the Laboratory Directed Research and Development Program at Sandia National Laboratories, which is by operated by Sandia Corporation, a Lockheed Martin Company, for the US Department of Energy (contract DE-AC04-94-AL85000).

Additional information

The authors declare no competing financial interests. Reprints and permission information is available online at http://npg.nature.com/reprints. Correspondence should be addressed to F.L. or A.A.T.

© 2011 Macmillan Publishers Limited. All rights reserved

ERRATUM

Electrical contacts to one- and two-dimensional nanomaterials

François Léonard and A. Alec Talin

Nature Nanotechnology http://dx.doi.org/10.1038/nnano.2011.196 (2011); published online 27 November 2011;
corrected online 28 November 2011.

In the version of this Review originally published online, equation (2) appeared incorrectly. This has now been corrected in all versions of the Review.

© 2011 Macmillan Publishers Limited. All rights reserved